Journal of Inorganic Biochemistry 162 (2016) 102–108

Contents lists available at ScienceDirect

Journal of Inorganic Biochemistry

journal homepage: www.elsevier.com/locate/jinorgbio

Theoretical investigation of the mechanism of nitroxyl decomposition in aqueous solution

Mauro Bringas [1], Jonathan Semelak [1], Ari Zeida, Dario A. Estrin *

DQIAyQF, INQUIMAE-CONICET, FCEN UBA, Ciudad Universitaria, Pab. 2, CP, 1428 Buenos Aires, Argentina

ARTICLE INFO

Article history:
Received 27 January 2016
Received in revised form 8 June 2016
Accepted 14 June 2016
Available online 15 June 2016

Keywords:
Nitroxyl
Reactive nitrogen species
Aqueous decomposition
Mechanism
QM/MM

ABSTRACT

Nitroxyl (HNO) is a species that has been proposed recently to play different roles in nitrosative stress processes. HNO decomposition in aqueous solution leading to N_2O is a fast reaction that competes with many biochemical reactions in which HNO may be involved. Since molecular determinants of this reaction are still not fully understood, we present in this work an exhaustive analysis of the mechanism in terms of electronic-structure calculations as well as *state of the art* hybrid quantum mechanics/molecular mechanics molecular dynamics simulations. We characterized the reaction mechanism and computed free energy profiles for the reaction steps using an umbrella sampling procedure. We propose a first dimerization step followed by an acid-base equilibria. Afterwards, the product is formed from two main pathways involving *cis*-hyponitrous acid (*cis*-HONNOH) and its conjugate basis as intermediate. Our calculations show preference for the anionic pathway under physiological conditions and allow us to rationalize the results in terms of a molecular description of specific interactions with the solvent. These interactions turn out to be determinant in the stabilization of transition states and, thereby, modifying the free energy barriers. We predict a strong pH-dependence of the overall kinetics of N_2O formation, related with the fraction of reactive species available in solution. Finally, we suggest experimental procedures which could validate this mechanism.

1. Introduction

Nitroxyl (HNO) and its conjugate base (NO^-) were added recently to the family of reactive nitrogen species (RNS) [1,2]. Nitroxyl is a simple yet biologically relevant molecule. Even though it was discovered in the XIXth century, many aspects of its reactivity and its biochemical role are still controversial or not fully understood [3]. Historically, HNO was considered as a biologically active molecule because of studies related with cyanamide (H_2NCN), which is used in alcoholism treatment [4,5]. Cyanamide reaction with catalases and peroxidases generates HNO, that reacts with a residue of cysteine (in thiolate form) in the active site of the aldehyde dehydrogenase, inhibiting it. This represents only one example among many of the high reactivity of HNO with thiolates (RS^-) [6–8].

Nitroxyl's potential use in heart failure treatment makes it relevant in the field of pharmacology, as well as its vasodilator properties and its role in cellular metabolisms [9,10].

Nitroxyl rapidly decomposes in aqueous solution generating nitrous oxide [11]. Due to its inherent reactivity and the need for in situ generation, the search of HNO donors and a better understanding of its chemical behavior have intensified considerably its biological interest.

[1,12] The first method developed for in situ generation of HNO was the decomposition of $Na_2N_2O_3$ (Angeli's salt), which is still used for this purpose. [13,14] Also, organic donors of HNO have been investigated, such as the Piloty's Acid (Benzenesulphonydroxamic acid) that yield HNO via heterolysis in alkaline conditions [15–17].

At the same time, an increase of physicochemical interest in the decomposition has taken place in the last years, with the aim of developing regulation strategies for this process. However, the reaction mechanism of this extremely relevant reaction is still not understood from a molecular viewpoint.

As a necessary feature to nitrous oxide formation an initial dimerization step has been proposed [18,19]. This implies the existence of a planar intermediate [20]:

$$2HNO \rightarrow cis\text{-}ON(H)N(H)O \rightarrow N_2O + H_2O \quad (1)$$

Because of a certain double bond character between the nitrogen atoms, the planar intermediate may exhibit two isomers: *cis*-ON(H)N(H)O and *trans*-ON(H)N(H)O and, once the dimer has been formed, *cis-trans* isomerization would be kinetically forbidden at moderate temperatures. This way, the initial dimer of HNO sets the starting point for the overall reaction.

After the initial dimer formation, a scheme involving intramolecular proton migrations has been proposed to explore different reaction mechanisms for the N_2O formation [20–22]. However, none of this

* Corresponding author.
E-mail address: dario@qi.fcen.uba.ar (D.A. Estrin).
[1] These authors made equal contributions.

http://dx.doi.org/10.1016/j.jinorgbio.2016.06.016
0162-0134/

treatments include explicit water molecules and realistic transition states with feasible structures that could exist in aqueous solution.

In agreement with the work of Fehling et al. [20], we propose that a fast acid-base equilibria takes place between the dimer formation and the final decomposition in N_2O. The solvent, H_2O, is clearly involved in the formation of different protonation states of the dimer so intramolecular proton migration scheme is probably not operative in aqueous solution. The global reaction could be decomposed in three phases: a first dimerization step forming the *N—N* bond with a given conformation (*cis* or *trans*), followed by a fast acid-base equilibria and finally, the N_2O formation step from a given intermediate.

It was also proposed that HNO decomposition may take place by a nucleophilic attack of NO^- to the nitrogen atom of HNO, followed by an 1.2 hydrogen transfer finally yielding N_2O and HO^- [23]. However, this mechanism is not considered in this work because of the high pKa of HNO (11.4) [11] and therefore the very low concentration of NO^- available at physiological pH.

In order to obtain information about the mechanism of the reaction under investigation and to obtain valid starting structures for further analysis, we performed electronic structure calculations using *Gaussian09* [24]. Aiming to understand the whole process in aqueous solution, we explored both reaction steps by means of hybrid quantum mechanics-molecular mechanics (QM/MM) molecular dynamics (MD) simulations, using an umbrella sampling approach [25]. This approach allowed us to obtain thermodynamical information such as the free energy profile in addition to microscopic insight about electronic structure changes throughout the reaction in a realistic solvent environment. The results presented in this work suggest that the process may occur by different pathways, by a strongly pH-dependent mechanism, since the rate constant would variate in approximately a 10^5 factor.

The data reported herein provides a detailed microscopic view of the nitroxyl decomposition in aqueous solution.

2. Methods

2.1. Initial survey of the system in vacuum and implicit solvent

All structures were optimized in vacuo and using the polarizable continuum solvent model (PCM) [26], at DFT level of theory. Computations were performed at the generalized gradient approximation (GGA) level, using the PBE combination of exchange and correlation functional, with a double-zeta plus polarization (dzvp) Gaussian basis set [27]. An auxiliary basis set was employed, frequency calculations were performed in each case and free energies were estimated by means of standard statistical mechanics formalisms. The PCM aqueous solvation default parameters have been employed.

The geometries obtained with this functional were used as the starting point for a first approximation of the energy profile of each reaction step using the PCM solvation model, in order to obtain partial charges necessary to perform the classical MD simulations which are required to equilibrate the systems, as described below. After this initial survey, we performed molecular dynamics simulations using a QM/MM scheme.

In addition, kinetics isotope effect analysis was performed by employing the harmonic oscillator and rigid rotor approximations for the zero point energies, vibrational and rotational contributions, using classical statistical mechanics as implemented in the Gaussian code (see Supplementary Information for a more detailed description) [28].

2.2. QM/MM molecular dynamics simulations

QM/MM simulations were performed using LIO, a software developed in our group [29]. The QM subsystem contained the nitroxyl dimer while the MM subsystem consisted only of water molecules. Free energy profiles were obtained by the umbrella sampling method [25]. Initial structures for the *cis*-ON(H)N(H)O were obtained from ab initio, PBE level, geometry optimizations. A truncated 20 Å octahedral box was constructed and filled with TIP4P model water molecules [30]. Periodic boundary conditions were used, and each box contained only one dimer molecule and 4100 explicit water molecules. The Lennard-Jones parameters (ε and σ) for the quantum subsystem atoms were 0.7113, 0.8803 and 0.0669 $kJ \cdot mol^{-1}$, and 1.8240, 1.7210 and 1.069 Å, for N, O, and H, respectively. The initial system optimization was carried out in two stages: first, solute was optimized freezing the classical water molecules. Secondly the solvent was optimized, keeping fixed the QM subsystem. 30 ns of classical thermalization dynamics were simulated, heating from 0 to 300 K, applying an internal motion restraint on the nitroxyl dimer. To ensure a reliable thermalization of the solute, 1 ps of QM/MM simulation was generated with an uncoupled Berendsen thermostat [31]. A stronger coupling constant was set for the QM system's thermostat. This double thermostat strategy provides an advantage in terms of controlling the local kinetic energy of such a small subsystem. A steered QM/MM molecular dynamics simulation was performed, forcing the QM system through the reaction coordinate, with the aim of extracting initial structures for subsequent umbrella sampling calculations. These structures, corresponding to different reaction coordinate values, were then thermalized in order to improve solvation sampling. A recalculation of the classical residue's charge was carried out after 0.1 ns of classical molecular dynamics simulation, holding the dimer still and then slightly optimized before partial charge calculations. This process was iteratively repeated 10 times. The process consisted on three stages: in the first place a single point calculation was performed for the solute and the charge parameters were modified in the classical residue parametrization. After that, a ten-step cycle was carried out. Each of these steps consisted on a 0.1 ns classical molecular dynamic simulation of the solvent, holding the solute still, and a short QM optimization for that new solvation scheme. Those optimized parameters were then used to modify the topology in each cycle. After this final thermalization, those structures were used as initial coordinates for each umbrella sampling window. For each window, 5 ps of uncoupled thermostat QM/MM molecular dynamics simulation were generated, followed by additional 10 ps using the stochastic Langevin thermostat model. Only Langevin MD information was used for the analysis. This combination of relatively long classical molecular dynamics simulations, in which the parameters are tuned at each reaction coordinate value, with shorter QM/MM simulations, allows us to obtain reliable free energy profiles at an affordable computational cost.

All dynamics visualizations and molecular drawings, were performed with VMD 1.9.1 [32].

3. Results and discussion

3.1. Reaction evolution

The first step of the reaction consists in the formation of a *N—N* bond between two HNO molecules, giving a planar intermediate which may exhibit two isomers (see Scheme 1). Table 1 presents the results of calculations for the initial dimerization step.

No transition state was found for the dimer formation reaction. When the solvent is taken into consideration, there is a switch in the relative stability of both isomers. Because of its non-zero dipole moment, the *cis* isomer is expected to be the most stable one in aqueous solution. Both our results and previous studies [20] give evidence that supports

Scheme 1. *cis* and *trans* representations of the dimer intermediate.

Table 1
Dimerization energies and free energies ($kJ \cdot mol^{-1}$) for isolated and PCM solvated species involved in the dimerization step, relative to 2 HNO molecules.

	Free energies		Energies	
	In vacuo	PCM	In vacuo	PCM
cis-ON(H)N(H)O	−109.3	−152.9	−138.9	−179.9
trans-ON(H)N(H)O	−121.9	−144.0	−152.6	−170.3

that the *cis* dimer is the most favorable adduct in aqueous solution. The free energy profile was obtained for the *cis*-dimer formation step (see Fig. 1). The reaction coordinate corresponds to the *N—N* bond length. The dimer formation turned out to be an exergonic step ($\Delta G \simeq -200\ kJ \cdot mol^{-1}$), as it is expected for this kind of bond formation reactions. No activation barrier was detected with this methodology just like in the QM survey via the PCM approach.

We propose that, once the *cis*-ON(H)N(H)O is formed, an acid-base equilibria takes place. The relative stabilities of the different protonation states of the $(HNO)_2$ dimer were calculated, both in vacuo and in implicit solvent. The *cis*-hyponitrite (*cis*-HONNOH) turned out to be the most stable tautomer, which is consistent with the work of Fehling et al. Table 2 summarizes the relative energies between dimer tautomers. It is the reasonable to assume that the N_2O formation takes place mainly from this intermediate, as:

$$cis-ON(H)N(H)O \leftrightarrows cis-HONNOH \rightarrow N_2O + H_2O \quad (2)$$

In order to estimate the reaction and the activation energy, a QM approach was carried out in the same way as for the first dimerization step. For this step, the structures of reactants complex (RC) (*cis*-HONNOH), products complex (PC) (N_2O/H_2O) and transition state (TS) were optimized.

As *cis*-HONNOH pKa has not been determined, it is unknown whether at physiological pH the reaction is going to proceed from the *cis*-HONNOH or from the [*cis*-HONNO]$^-$. In order to evaluate both conditions, we considered that the reaction could either take place from *cis*-HONNOH (a "neutral pathway"), or undergo an "anionic pathway", in which the reactive species for the second step is the single protonated *cis*-hyponitrite, [*cis*-HONNO]$^-$. This anionic mechanism would yield N_2O and HO^- as products. Relative energies for both pathways are shown in Table 3.

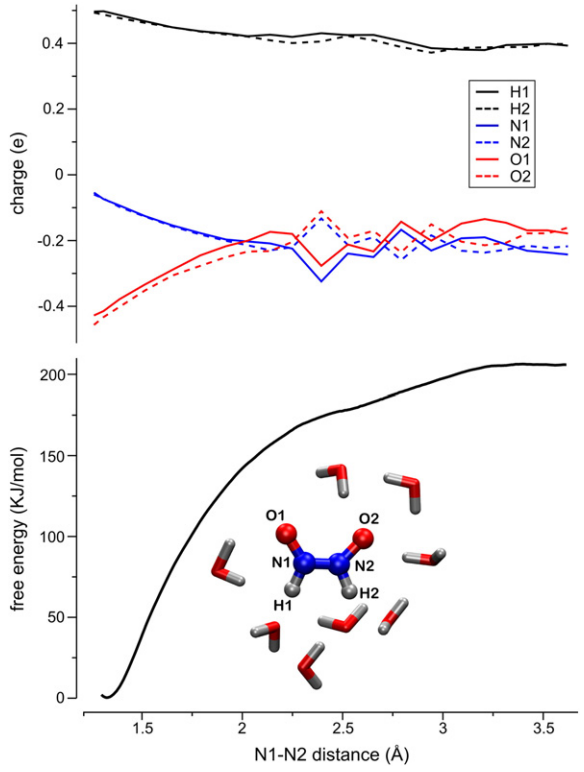

Fig. 1. Free energy profile and Mulliken charges for each QM susbsystem atom as a function of the reaction coordinate ($kJ \cdot mol^{-1}$ and e, respectively). An illustrative snapshot of the RC and its first solvation shell is also shown.

Table 2
Energies and free energies ($kJ \cdot mol^{-1}$) for isolated and PCM solvated tautomeric species of $(HNO)_2$ relative to *cis*-ON(H)N(H)O.

	Free energies		Energies	
	In vacuo	PCM	In vacuo	PCM
trans-ON(H)N(H)O	12.6	8.9	−13.7	9.6
cis-HONNOH	−78.1	−47.4	−76.8	−43.3
trans-HONNOH	−58.6	−29.6	−57.4	−25.8
cis-ON(H)NOH	−68.4	−39.2	−71.2	−39.4
trans-ON(H)NOH	−36.6	−12.3	−35.5	−9.3
cis-ONN(H)OH	−58.3	−34.8	−57.2	−26.4
trans-ONN(H)OH	−26.1	−1.8	−19.9	8.5

It was not possible to optimize the structure of PC and TS in vacuum for the anionic pathway. We found that the inclusion of the environment by PCM has a significant effect on all models used herein. In fact, only via the PCM approach we could study the energetics involved in the anionic pathway.

A kinetic isotope effect analysis was carried out by replacing N_2 and O_2 atoms by their heavy isotopes (N^{15} and O^{18}) as previously described. Single substitutions retrieved a negligible difference in their kinetic constants estimated by Eyring's equation. However, double isotope substitution for both N_2 and O_2 (see Table 3) exhibited a significant $\Delta\Delta G_{act}$, which meant a 3% and 10% decrease in the calculated rates for both neutral and anionic pathways, respectively.

In order to obtain microscopic insight of the reaction mechanism, key geometric parameters of different states of the process were analyzed (see Table 4). Even though N_2-O_2 distance in RC and PC is nearly the same for both pathways, in the TS the difference is clear. In the neutral pathway, the N_2-O_2 distance seems to indicate an early TS, while in the anionic pathway the geometric parameters indicate a late one. This is a key difference between our QM/MM analysis and this implicit solvent QM approach. This product-like transition state is not observed in our QM/MM calculations, where the anionic pathway TS geometry still resembles the RC. On the other hand, N_2-O_2 distance predicted for neutral pathway for both methodologies is approximately the same, since the free energy profile reaches its maximum between 1.8 and 1.9 Å. Similar activation barriers for both pathways were determined with the QM calculations. Nevertheless, despite the expectation of an exergonic process, only the neutral pathway shows a negative free energy change within this QM scheme. A stronger solvation stabilization effect would be expected for the product complex in the anionic mechanism respect to the neutral one, retrieving a higher reaction free energy difference. This fact is not a surprise, since it is known that the implicit solvent does not model properly hydrogen bonding interactions, which may be crucial for charged species. Our QM/MM approach allows us to obtain a more realistic picture of solvation in bulk water at room temperature. So, in order to obtain free energy profiles for this

Table 3
Relative Energies and Free Energies ($kJ \cdot mol^{-1}$) for isolated and PCM solvated species involved in the N_2O formation from *cis*-HONNOH and [*cis*-HONNO]$^-$. Isotopic effect free energy activation barrier ($\Delta\Delta G_{act}$) variation for substitution of N2 to N^{15} and O2 to O^{18} is also shown.

		ΔE_{react}	E_{act}	ΔG_{react}	ΔG_{act}	$\Delta\Delta G_{act}$
Neutral pathway	*In vaccuo*	−114.9	69.3	−136.7	57.6	–
	PCM	−112.6	70.0	−136.3	59.2	0.06
Anionic pathway	*In vaccuo*	–	–	–	–	–
	PCM	82.6	84.1	64.6	66.6	0.25

Table 4
Relevant geometric parameters (distances in Å and angles in degrees) of Reactant Complex (RC), Transition State (TS) and Product Complex (PC) of both Neutral and Anionic Pathways (NP and NA, respectively), obtained from PCM optimized structures.

		d(N2-O2)	d(N1-N2)	d(O2-H2)	angle(N2-N1-O1)
RC	NP	1.42	1.25	1.89	116
	AP	1.44	1.42	–	118
TS	NP	1.88	1.20	1.27	125
	AP	2.75	1.46	–	168
PC	NP	3.19	1.16	0.98	180
	AP	3.11	1.16	–	177

step, we performed QM/MM simulations as described above for the dimerization step.

The reaction coordinate for this process corresponds to the N_2-O_2 distance, which leads the reactant complex to nitrous oxide and water or hydroxide ion. The free energy profiles are shown in Fig. 2, along with the evolution of other parameters of interest during the reaction (for the neutral pathway, see Fig. S1). The anionic pathway retrieved a smaller barrier, exhibiting a $\Delta G^{act} \simeq 30$ kJ·mol^{-1} versus a $\simeq$ 60 kJ·mol^{-1} energy barrier for the neutral pathway. In other words, the explicit solvent consideration diminishes the activation barrier of the anionic pathway. Our QM/MM scheme allowed us to find a more feasible path for the N_2O formation step than the typically *cis*-HONNOH.

Even though the neutral pathway exhibits a larger barrier, this mechanism is expected to be relevant at low pH values, because of the increase of the fully *O*-protonated species concentration. So, the contributions of the different pathways to the global N_2O production will be modulated by pH, with smaller reaction rates at low pH values, at which the neutral pathway is the main mechanism. pH-dependence of the global rate constant has been reported previously for *trans*-hyponitrous acid (*trans*-HONNOH) decomposition by Buchholz and Powell, that showed a decrease of the rate constant from pH 9 to 1 which was interpreted in terms of available reactive species ([*trans*-HONNO]-) population decrease [33].

The TS for the anionic-pathway exhibits a 140° N1-*N*-O_2 angle. The activation barrier seems to be concomitant with a strong charge redistribution of N and O atoms, where N_1 and O_1 become more positive, as well as N_2 and O_2 acquire negative charge (see Fig. 2)

Electronic structure calculations for *cis*-*trans* isomerization of $(HNO)_2$ species performed in literature showed high energy barriers that cannot compete with proton transfer processes and the decomposition itself [20]. This is consistent with the high stability of *trans*-HONNOH, whose decomposition rate reaches a maximum of 5×10^{-4} s^{-1}, at pH = 9 [33]. A remaining question is what occurs to the HNO that undergoes a *trans*-pathway in the initial step, yielding *trans*-ON(H)N(H)O.

In the context of the fast acid-base equilibrium scheme, the *trans*-ON(H)N(H)O and its tautomers will be established rapidly and should probably experiment an analogous decomposition mechanism, via the [*trans*-HONNO]$^-$ intermediate. A free energy barrier of 64.1 kJ·mol^{-1} for this last reaction step was estimated by electronic-structure calculations in a continuum solvent model, as was described in Section 2.1. However, we have focused our analysis in the *cis*-pathway due to the preference of *cis*-ON(H)N(H)O formation in the initial dimerization step. The quotient of the kinetic rates for *cis* and *trans* dimer formation was estimated to be 500 [20].

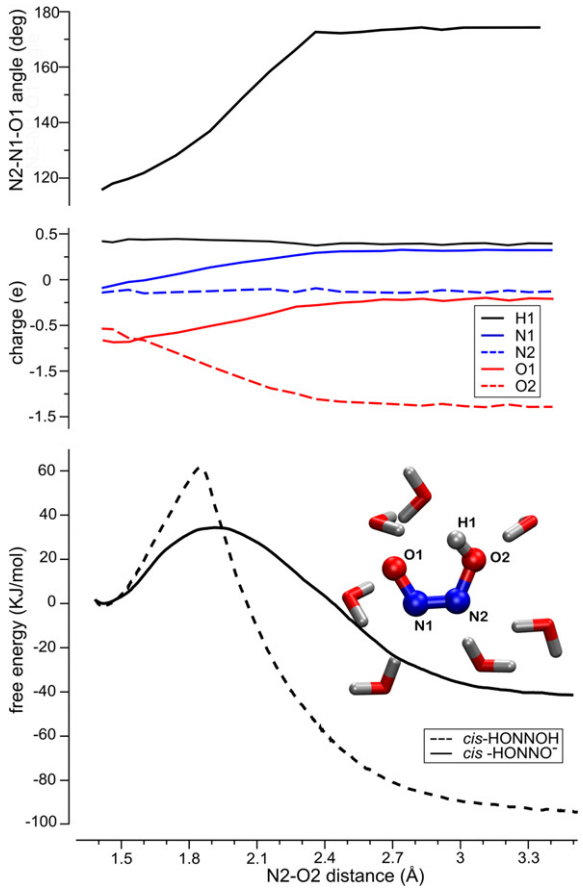

Fig. 2. Free energy profile obtained by umbrella sampling for the anionic (solid line) and the neutral (dashed line) pathway. N1-N2-O1 angle and charge evolution during the reaction from [cis-HONNO]$^-$ to N_2O and HO^-. Free energy (kJ·mol^{-1}) is plotted versus reaction coordinate (Å) as well as the Mulliken charges (e) and the N1-N2-O1 angle. An illustrative snapshot of the TS and its first solvation shell is also shown.

3.2. Solvation

We studied the solvation of RC, TS and PC to monitor how solvation patterns may affect the reaction energetics. Radial correlation functions of selected atoms with water oxygen atoms from the anionic pathway RC (left panel), TS (middle panel) and PC (right panel), along with representative snapshots of each step, are shown in Fig. 3 (solvation profiles for the neutral pathway are shown in Fig. S2). Radial correlation functions of O atoms show that the O1 loses its hydrophilicity along the reaction and the opposite effect is observed in the O2. While in the RC the O2 is poorly solvated, it becomes better solvated in the TS due to the early charges redistribution and strongly solvated in the PC. Moreover, the peaks of O2 curve observed in the TS and PC are located at ≃2.5 Å (radial distance), while the O1 curve peak in the RC is at about 2.8 Å. Radial correlation function value of O1 is lower than the one of the O2 in the TS, and even more in the PC. This is consistent with the charge evolution profile, which shows that O2 becomes more negative along the reaction. This suggests that the PC is much better solvated than the RC and the TS.

Radial correlation functions of N2 atom do not change significantly during the process, and N1 atom acquires a more effective solvation which is in the increase of radial correlation function value in its peaks. Both results are consistent with the redistribution of charges during the reaction, where N1 almost does not change its charge and N2 becomes more positive. An explicit aqueous environment in the TS and the PC provides a more realistic description of O2 in those situations, specific solvent stabilization effects which are not exhibited in a PCM approach.

This way, although water molecules are not involved as reactants in the mechanism, their explicit inclusion by an MM approach allow us to interpret the activation barrier in terms of changes in charges and solvation patterns during the process.

3.3. The reaction mechanism and available experimental information

The global reaction mechanism can be written as a consecutive reactions scheme with quick acid-base equilibria which connect products

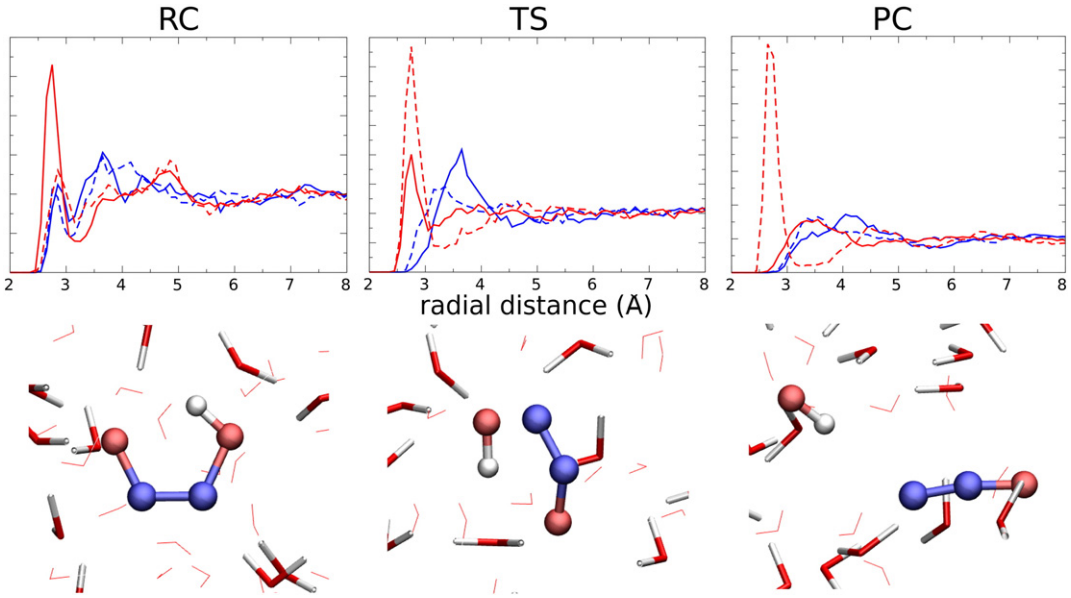

Fig. 3. Solvation structure evolution for the anionic pathway. Up: radial correlations functions of nitrogen (blue) and oxygen (red) in solid (1) and dashed (2) lines with water oxygen atoms from the RC (left panel), TS (middle panel) and PC (right panel). Down: representative snapshots of the solvation structure of the RC (left panel), TS (middle panel) and PC (right panel).

and reactants of different steps:

$$\begin{aligned} 2HNO &\xrightarrow{k_1} cis{-}ON(H)N(H)O \\ cis{-}ON(H)N(H)O &\leftrightarrows cis{-}HONNOH \\ cis{-}HONNOH &\leftrightarrows [cis{-}HONNO]^- + H^+ \\ cis{-}HONNOH &\xrightarrow{k_2^{NP}} N_2O + H_2O \\ [cis{-}HONNOH]^- &\xrightarrow{k_2^{AP}} N_2O + HO^- \end{aligned} \tag{3}$$

Where k_1, k_2^{NP} and k_2^{AP} are the constants for the dimerization and the dimer dissociation via the neutral and anionic pathway elemental steps, respectively. k_1, can be expected to be, as much, in the order of diffusion controlled reactions rate ($\approx 10^9$ M^{-1} s^{-1}) whereas a k_2^{AP} value of 4×10^7 s^{-1} can be calculated from Eyring equation using the free energy barrier obtained from our QM/MM simulations. Same way, a 2×10^2 s^{-1} value was estimated for N_2O formation elemental step in the neutral pathway (k_2^{NP}). The equilibrium between *cis*-ON(H)N(H)O and *cis*-HONNOH is characterized by a predicted free energy difference of -43.7 kJ·mol^{-1} (see Table 2). However, *cis*-$(HNO)_2$ tautomers pKa have not been measured and the computational predictions may be very dependent on the electronic structure level of theory and solvation model.

In order to contrast our results with experimental data available, it is necessary to review the information given in the literature about the rate constant of HNO decomposition in aqueous solution. Previously, Bazylinski et al. [34] reported a rate constant of 2×10^9 M^{-1} s^{-1}, suggesting a diffusional control for the HNO decomposition reaction. This constant was determined from Angeli's Salt [13,14] decomposition at pH = 7.0 in presence of excess ^{15}NO, and calculations were carried out taking a HNO pKa of 4.7 [35]. This pKa value was corrected to be of 11.4 some years later by Shafirovich and coworkers [11] and in the same work a rate constant of 8×10^6 M^{-1} s^{-1} was reported, which was determined from flash-fotolysis peroxinitrite formation, fitting the HNO concentration decrease detected in strongly alkaline conditions ($11 < pH < 13$). In this last experiment, HNO was generated in a time scale in which its acid-base equilibrium does not affect the HNO dimerization process, since the HNO deprotonation is a spin-forbbiden reaction and then, slow ($k = 4.9 \times 10^4$ M^{-1} s^{-1}). Considering this, the rate constant determined turns out to be pH-independent. Although this value is commonly cited in literature as the HNO dimerization rate constant, our results suggest that the global mechanism is governed by pH, so it is important to analyze if it could be generalized to lower pH (and particularly to physiological pH). This dependence is introduced by the $(HNO)_2$ acid-base equilibrium, required to yield the reactive tautomers.

First, it is important to remark that in Shafirovich's experiment [11], HNO consumption is indirectly followed and attributed to its decomposition in aqueous solution. This way, the 8×10^6 M^{-1} s^{-1} rate constant corresponds, in our scheme, with k_1. According to our calculations, this rate would be diffusional, and differences with our calculations may be related to flaws in DFT methodologies, which could be underestimating free energy barriers and also probably flaws in the experimental data analysis, since the rate constant was determined in an indirect way and with several assumptions. Another question that arises is if the rate of HNO consumption is equal to the rate of N_2O formation. From the mass balance of nitrogen, we obtain:

$$0 = \frac{d[HNO](t)}{dt} + 2\frac{d[(HNO)_2](t)}{dt} + 2\frac{d[N_2O](t)}{dt}, \tag{4}$$

where $[(HNO)_2](t)$ represents the total dimer concentration at time t. It can be seen that only if $d[(HNO)_2](t)/dt \approx 0$ the N_2O formation rate approximately equals to HNO disappearance rate. In other words, there will not exist intermediate ($(HNO)_2$) accumulation if we assume the *steady-state* approximation. To study this possibility, it is necessary to solve the differential equations which describe the kinetics of the process and then compare the analytical solution with that obtained under this approximation. An alternative way for solving this problem is to integrate numerically the kinetic equations and fit the rate constants using experimental data, which is not currently available.

In the light of the previously discussed, the commonly used rate constant can be effectively extrapolated to lower pH because it corresponds to HNO consumption. On the other hand, this proposed mechanism suggests that N_2O formation is a strongly pH-dependent process, with an effective constant rate:

$$k_2^{eff} = \alpha_{[cis-HONNO^-]} k_2^{AP} + \alpha_{cis-HONNOH} k_2^{NP}, \tag{5}$$

where $\alpha_{[cis-HONNO^-]}$ and $\alpha_{cis-HONNOH}$ are the fractions of *cis*-$(HNO)_2$ in each reactive form and weights both calculated microscopic rate

constants (see Fig. S4). Fehling et al. have estimated theoretically pKa values for $(HNO)_2$ tautomers by means of DFT calculations in an implicit solvent approach [20]. Using these estimations of pKa for *cis*-ON(H)N(H)O and *cis*-HONNOH (−2.6 and 3.1, respectively) and relative free energies from our calculations of *cis*-$(HNO)_2$ species (see Table 2), we calculated their relative concentrations as a function of pH (see Fig. S3). pKa of [*cis*-HONNO]$^-$ is expected to be around 17 [20] and so the double charged specie [*cis*-ONNO]$^{2-}$ is neglected in our analysis.

We confirmed the *cis*-HONNOH and [*cis*-HONNO$^-$] predominate even in alkaline conditions. However, we are only interested in pH values lower than 9, where NO^- is negligible (HNO pKa = 11.4) [11]. The speciation diagram for the *cis*-$(HNO)_2$ shows two regions in which each reactive dimer predominates over the other species where, particularly, [*cis*-HONNO$^-$] predominates from pH ≃ 5 onwards.

It can be seen that the anionic pathway will be the only one operative from pH ≃ 5 onwards. This would be the case if the difference between *cis*-ON(H)N(H)O and *cis*-HONNOH pKa was large.

In this context, N_2O formation rate constant as a function of pH, a sigmoideal-like dependence should be obtained, with two *plateaus* in k_2^{eff} which should differ roughly in a 10^5 factor. Moreover, since $(HNO)_2$ species are practically negligible versus *cis*-HONNOH and [*cis*-HONNO]$^-$ (see Fig. S3), a numerical fitting of the curve would yield also a good approximation to the pKa value of *cis*-HONNOH. Our estimated k_2^{eff} as function of pH is shown in Fig. S4. Regarding possible experiments carried out in heavy water, the observed kinetic isotope effect for the anionic pathway would probably be analogous to the reported by Buchholtz and Powell [33] since there is no hydrogen-heavy atom bond cleavage. In this context of *cis*-isomer studies, a decrease in the rate constant due to hydrogen substitution by deuterium would be mainly observed in the neutral pathway, where a hydrogen (or deuterium) transfer is part of the mechanism. The previously proposed experiment to determine an effective value for k_2, performed for a wide range of pH values, should retrieve a different curve. The value of k_2 in D_2O would be different to the one in H_2O, retrieving a different value for k_2^{eff} both the low-pH and the high-pH region. Our electronic structure calculations predict a 3.37 value for the rate $k_2^{NP}(H_2O)/k_2^{NP}(D_2O)$. In addition, all *cis* tautomers and monoanionic forms' pKa would be modified due to the isotope substitution, and this would result in an additional horizontal shift of the k_2^{eff} sigmoideal-like curve.

4. Conclusions

In this work we present an integrated QM/MM approach for nitroxyl decomposition, which allows us to get microscopic dynamical information of this reaction emphasizing the aqueous environment relevance.

This microscopic insight allowed us to obtain a consistent mechanism for the overall reaction. The initial step consists in *cis*-ON(H)N(H)O formation, followed by an acid-base equilibria. The *cis*-HONNOH species showed the highest stability compared to the other plausible tautomers and because of that we consider it a potential intermediate for the N_2O formation step. The, we consider the evidence presented herein suggests that the final step of this reaction may take place from both neutral and monoanionic forms of the HONNOH, with the monoanionic species being the most reactive [*cis*-HONNO]$^-$, given its lower activation free energy respect to the neutral species.

In addition, our results hold that the global process would pH-dependent. Further efforts in experimental investigations of this reaction are necessary to fully understand this issue.

Abbreviations

QM/MM	quantum mechanics/molecular mechanics
MD	molecular dynamics
DFT	density functional theory
PCM	polarizable continuum model
dzvp	double zeta plus polarization
AP and NP	anionic pathway and neutral pathway, respectively
RC, TS and PC	reactant complex, transition state and products complex, respectively

Acknowledgments

This work was supported by the Universidad de Buenos Aires (20020130100097BA UBACyT grant) and CONICET (PICT 2012-1266 and PICT 2014-1022 grants).

Appendix A. Supplementary data

Supplementary data to this article can be found online at http://dx.doi.org/10.1016/j.jinorgbio.2016.06.016.

References

[1] K.M. Miranda, The chemistry of nitroxyl (HNO) and implications in biology, Coord. Chem. Rev. 249 (3) (2005) 433–455.
[2] F. Doctorovich, D. Bikiel, J. Pellegrino, S.A. Suárez, A. Larsen, M.A. Martí, Nitroxyl (azanone) trapping by metalloporphyrins, Coord. Chem. Rev. 255 (23) (2011) 2764–2784.
[3] Y. Zhang, Computational investigations of HNO in biology, J. Inorg. Biochem. 118 (2013) 191–200.
[4] E.C. DeMaster, F.N. Shirota, H.T. Nagasawa, The metabolic activation of cyanamide to an inhibitor of aldehyde dehydrogenase is catalyzed by catalase, Biochem. Biophys. Res. Commun. 122 (1) (1984) 358–365.
[5] E.G. DeMaster, H. Nagasawa, F. Shirota, Metabolic activation of cyanamide to an inhibitor of aldehyde dehydrogenase in vitro, Pharmacol. Biochem. Behav. 18 (1983) 273–277.
[6] E.G. DeMaster, F.N. Shirota, H.T. Nagasawa, Catalase mediated conversion of cyanamide to an inhibitor of aldehyde dehydrogenase, Alcohol 2 (1) (1985) 117–121.
[7] E.G. DeMaster, B. Redfern, H.T. Nagasawa, Mechanisms of inhibition of aldehyde dehydrogenase by nitroxyl, the active metabolite of the alcohol deterrent agent cyanamide, Biochem. Pharmacol. 55 (12) (1998) 2007–2015.
[8] J.A. Reisz, E. Bechtold, S.B. King, Oxidative heme protein-mediated nitroxyl (HNO) generation, Dalton Trans. 39 (22) (2010) 5203–5212.
[9] X.L. Ma, F. Gao, G.-L. Liu, B.L. Lopez, T.A. Christopher, J.M. Fukuto, D.A. Wink, M. Feelisch, Opposite effects of nitric oxide and nitroxyl on postischemic myocardial injury, Proc. Natl. Acad. Sci. 96 (25) (1999) 14617–14622.
[10] K.M. Miranda, T. Katori, C.L. Torres de Holding, L. Thomas, L.A. Ridnour, W.J. McLendon, S.M. Cologna, A.S. Dutton, H.C. Champion, D. Mancardi, et al., Comparison of the NO and HNO donating properties of diazeniumdiolates: primary amine adducts release HNO in vivo, J. Med. Chem. 48 (26) (2005) 8220–8228.
[11] V. Shafirovich, S.V. Lymar, Nitroxyl and its anion in aqueous solutions: spin states, protic equilibria, and reactivities toward oxygen and nitric oxide, Proc. Natl. Acad. Sci. 99 (11) (2002) 7340–7345.
[12] K.M. Miranda, H.T. Nagasawa, J.P. Toscano, Donors of HNO, Curr. Top. Med. Chem. 5 (7) (2005) 649–664.
[13] A. Angeli, Sopra la nitroidrossilammina, Gazz. Chim. Ital. 26 (1896) 17–25.
[14] A. Angeli, F. Angelico, Nitrohydroxylaminic acid, Gazz. Chim. Ital. 33 (1903) 245–252.
[15] O. Piloty, Ueber eine oxydation des hydroxylamins durch benzolsulfochlorid, Ber. Dtsch. Chem. Ges. 29 (2) (1896) 1559–1567.
[16] P.C. Wilkins, H.K. Jacobs, M.D. Johnson, A.S. Gopalan, Mechanistic variations in the oxidation of piloty's acid by metal complexes, Inorg. Chem. 43 (24) (2004) 7877–7881.
[17] A. Porcheddu, L. De Luca, G. Giacomelli, A straightforward route to pilotys acid derivatives: A class of potential nitroxyl-generatingprodrugs, Synlett 2009 (13) (2009) 2149–2153.
[18] O. Strausz, H. Gunning, Reaction of hydrogen atoms with nitric oxide, Trans. Faraday Soc. 60 (1964) 347–358.
[19] F. Kohout, F. Lampe, On the role of the nitroxyl molecule in the reaction of hydrogen atoms with nitric oxide, J. Am. Chem. Soc. 87 (24) (1965) 5795–5796.
[20] C. Fehling, G. Friedrichs, Dimerization of HNO in aqueous solution: An interplay of solvation effects, fast Acid–Base equilibria, and intramolecular hydrogen bonding? J. Am. Chem. Soc. 133 (44) (2011) 17912–17922.
[21] M. Lin, Y. He, C. Melius, Theoretical interpretation of the kinetics and mechanisms of the HNO + HNO and HNO + 2NO reactions with a unified model, In. J. Chem. Kinet. 24 (5) (1992) 489–516.
[22] K. Ruud, T. Helgaker, E. Uggerud, Mechanisms, energetics and dynamics of a key reaction sequence during the decomposition of nitromethane: HNO + HNO → N_2O + H_2O, J. Mol. Struct. THEOCHEM 393 (1) (1997) 59–71.
[23] S.V. Lymar, V. Shafirovich, Photoinduced release of nitroxyl and nitric oxide from diazeniumdiolates, J. Phys. Chem. B 111 (24) (2007) 6861–6867.
[24] M. Frisch, G. Trucks, H. Schlegel, G. Scuseria, M. Robb, J. Cheeseman, G. Scalmani, V. Barone, B. Mennucci, G. Petersson, et al., Gaussian 09, Gaussian, Inc., Wallingford, CT, 2009.
[25] J.M. Rosenbergl, The weighted histogram analysis method for free-energy calculations on biomolecules. I. The method, J. Comput. Chem. 13 (8) (1992) 1011–1021.

[26] J. Tomasi, B. Mennucci, R. Cammi, Quantum mechanical continuum solvation models, Chem. Rev. 105 (8) (2005) 2999–3094.
[27] N. Godbout, D.R. Salahub, J. Andzelm, E. Wimmer, Optimization of Gaussian-type basis sets for local spin density functional calculations. Part I. Boron through neon, optimization technique and validation, Can. J. Chem. 70 (2) (1992) 560–571.
[28] F. Westheimer, The magnitude of the primary kinetic isotope effect for compounds of hydrogen and deuterium, Chem. Rev. 61 (3) (1961) 265–273.
[29] M.A. Nitsche, M. Ferreria, E.E. Mocskos, M.C.G. Lebrero, GPU accelerated implementation of density functional theory for hybrid QM/MM simulations, J. Chem. Theory Comput. 10 (3) (2014) 959–967.
[30] W.L. Jorgensen, J. Chandrasekhar, J.D. Madura, R.W. Impey, M.L. Klein, Comparison of simple potential functions for simulating liquid water, J. Chem. Phys. 79 (2) (1983) 926–935.
[31] H.J. Berendsen, J.P.M. Postma, W.F. van Gunsteren, A. DiNola, J. Haak, Molecular dynamics with coupling to an external bath, J. Chem. Phys. 81 (8) (1984) 3684–3690.
[32] W. Humphrey, A. Dalke, K. Schulten, VMD: visual molecular dynamics, J. Mol. Graph. 14 (1) (1996) 33–38.
[33] J.R. Buchholz, R.E. Powell, The decomposition of hyponitrous acid. I. The non-chain reaction, J. Am. Chem. Soc. 85 (5) (1963) 509–511.
[34] D.A. Bazylinski, T.C. Hollocher, Evidence from the reaction between trioxodinitrate (II) and nitrogen-15-labeled nitric oxide that trioxodinitrate (II) decomposes into nitrosyl hydride and nitrite in neutral aqueous solution, Inorg. Chem. 24 (25) (1985) 4285–4288.
[35] M. Graetzel, S. Taniguchi, A. Henglein, Pulse radiolytic study of short-lived by-products of nitric oxide-reduction in aqueous solution, Ber. Bunsen Ges. 74 (1) (1970) 1003–1010.